THE JOURNAL OF BIOLOGICAL CHEMISTRY VOL. 281, NO. 24, pp. 16785–16793, June 16, 2006

The Structure of G Protein-coupled Receptor Kinase (GRK)-6 Defines a Second Lineage of GRKs*[S]

Received for publication, February 10, 2006, and in revised form, March 29, 2006 Published, JBC Papers in Press, April 13, 2006, DOI 10.1074/jbc.M601327200

David T. Lodowski[‡], Valerie M. Tesmer[‡§], Jeffrey L. Benovic[¶], and John J. G. Tesmer[‡§1]

From the [‡]Department of Chemistry and Biochemistry, Institute for Cellular and Molecular Biology, University of Texas, Austin, Texas 78712-0165, the [§]Life Sciences Institute, Department of Pharmacology, University of Michigan, Ann Arbor, Michigan 48109-2216, and the [¶]Department of Biochemistry and Molecular Biology, Kimmel Cancer Center, Thomas Jefferson University, Philadelphia, Pennsylvania 19107

We describe the 2.6-Å crystal structure of human G protein-coupled receptor kinase (GRK)-6, a key regulator of dopaminergic signaling and lymphocyte chemotaxis. GRK6 is a member of the GRK4 subfamily of GRKs, which is represented in most, if not all, metazoans. Comparison of GRK6 with GRK2 confirms that the catalytic core of all GRKs consists of intimately associated kinase and regulator of G protein signaling (RGS) homology domains. Despite being in complex with an ATP analog, the kinase domain of GRK6 remains in an open, presumably inactive conformation, suggesting that G protein-coupled receptors activate GRKs by inducing kinase domain closure. The structure reveals a putative phospholipid-binding site near the N terminus of GRK6 and structural elements within the kinase substrate channel that likely influence G protein-coupled receptor access and specificity. The crystalline GRK6 RGS homology domain forms an extensive dimer interface using conserved hydrophobic residues distinct from those in GRK2 that bind $G\alpha_q$, although dimerization does not appear to occur in solution and is not required for receptor phosphorylation.

G protein-coupled receptor kinases (GRKs)[2] initiate homologous desensitization by phosphorylating the third cytoplasmic loop or tail of activated G protein-coupled receptors (GPCRs) (1, 2), thereby allowing cells to adapt to changing extracellular signals. The seven mammalian GRKs are grouped into three subfamilies based on sequence identity and gene structure (3). The GRK1 subfamily consists of rhodopsin kinase (GRK1) and GRK7; the GRK2 subfamily consists of β-adrenergic receptor kinase-1 and -2 (GRK2 and GRK3); and the GRK4 subfamily consists of GRK4–6. All GRKs have an ~500-amino acid structural core consisting of a regulator of G protein signaling (RGS) homology (RH) domain (4) and a kinase domain closely related to those of other AGC family members (5), including protein kinase A (PKA) and protein kinase B (PKB). However, each GRK subfamily has distinct N and C termini containing elements known to regulate kinase activity and to mediate membrane targeting (1, 6–8). The GRK2 and GRK4 subfamilies diverged >1 billion years ago and are present in most, if not all, metazoans, including *Drosophila melanogaster* and *Caenorhabditis elegans* (3). The GRK1 subfamily is thus far found only in vertebrates.

To date, the defining structural features of the GRK family have been surmised primarily through crystal structures of only one member, bovine GRK2. In the crystal structures of GRK2 (9) and its complexes with $G\beta\gamma$ (10) and $G\alpha_q$ (11), the RH and kinase domains of GRK2 are intimately associated via a bipartite interaction that is reminiscent of the inhibited structures of Src family tyrosine kinases (12–14). In each structure, the kinase domain of GRK2 adopts an open, presumably inactive conformation similar to that of the open state of PKA (15). Remarkably, the GRK2 RH domain has two additional protein interaction sites. The first binds the C-terminal pleckstrin homology (PH) domain of GRK2, by which the enzyme is recruited to the membrane via binding activated $G\beta\gamma$ subunits (16–18), and the second binds activated $G\alpha_q$ subunits (19–22). Based on how PH domains and $G\beta\gamma$ are expected to associate with lipid bilayers, a membrane-bound orientation was proposed for GRK2 (10). However, it was not known if the structural and functional correlates established for GRK2 necessarily apply to the other GRK subfamilies, which do not have PH domains and are not known to bind directly to $G\alpha$ subunits (19). Whereas the GRK kinase domain is relatively well conserved among the subfamilies (~45% sequence identity), the RH domain is much less so (~27% identity), and the GRK N and C termini have little or no sequence homology. Therefore, the structure and interdomain contacts of the RH-kinase domain core, the kinase domain conformation, and the membrane orientation in other GRK subfamilies could be substantially different. Moreover, it is not clear whether the RH domains of GRK1 and GRK4 subfamily members will serve a role in mediating intermolecular protein-protein interactions.

To address these issues, we determined the 2.6-Å crystal structure of GRK6, the most ubiquitously expressed member of the GRK4 subfamily (3, 23–25). Physiological roles of GRK6 include regulating dopamine, M_3 muscarinic, opioid, and chemokine receptor signaling (26–32). GRK6 is also thought to play maladaptive roles in addiction (28) and Parkinson disease (28, 29), and as such, GRK6 represents a potential therapeutic drug target. Unlike any of the GRK2 structures, the GRK6 crystal structure was determined in complex with AMPPNP, illuminating details of the GRK active site that may be important for the devel-

* This work was supported by American Heart Association Scientist Development Grant 0235273N, National Institutes of Health Grant HL071818, American Cancer Society Research Scholar Grant 04-185-01, and a Research Corporation Cottrell Scholar grant (to J. J. G. T.) and by National Institutes of Health Grant GM44944 (to J. L. B.). The work performed at the Advanced Light Source was supported by Contract DE-AC03-76SF00098 from the Office of Science, Office of Basic Energy Sciences, Materials Sciences Division, United States Department of Energy (to the Lawrence Berkeley National Laboratory). Proteomics data were provided by the Michigan Proteome Consortium (available at www.proteomeconsortium.org), which is supported in part by the Michigan Life Sciences Corridor. The costs of publication of this article were defrayed in part by the payment of page charges. This article must therefore be hereby marked "*advertisement*" in accordance with 18 U.S.C. Section 1734 solely to indicate this fact.

[S] The on-line version of this article (available at http://www.jbc.org) contains supplemental Figs. S1 and S2 and supplemental Refs. 1 and 2.

The atomic coordinates and structure factors (code 2ACX) have been deposited in the Protein Data Bank, Research Collaboratory for Structural Bioinformatics, Rutgers University, New Brunswick, NJ (http://www.rcsb.org/).

[1] To whom correspondence should be addressed: Life Sciences Inst., Dept. of Pharmacology, University of Michigan, 210 Washtenaw Ave., Ann Arbor, MI 48109-2216. Tel.: 734-615-9544; Fax: 734-763-6492; E-mail: johntesmer@umich.edu.

[2] The abbreviations used are: GRKs, G protein-coupled receptor kinases; GPCRs, G protein-coupled receptors; RGS, regulator of G protein signaling; RH, RGS homology; PKA, protein kinase A; PKB, protein kinase B; PH, pleckstrin homology; AMPPNP, 5′-adenylyl β,γ-imidodiphosphate; IP_3, inositol 1,4,5-trisphosphate; GSK3β, glycogen synthase kinase-3β.

Supplemental Material can be found at: http://www.jbc.org/cgi/content/full/M601327200/DC1

opment of GRK-selective kinase inhibitors. We compare the arrangement of the RH and kinase domains of GRK6 with those of GRK2 and assess the significance of an extensive, hydrophobic dimer interface formed by the GRK6 RH domain. One end of the predicted peptide-binding channel of GRK6 appears to be blocked by a loop within its kinase domain, and a putative phospholipid-binding site is revealed near the N terminus of the enzyme.

EXPERIMENTAL PROCEDURES

Expression and Purification of GRK6—To ensure a homogeneous preparation of GRK6 and to eliminate the need for detergent during the protein purification, human GRK6 was expressed in both Sf9 and High5 insect cells as a soluble, palmitoylation-deficient mutant in which three potential palmitoylation sites (located at Cys^{561}, Cys^{562}, and Cys^{565}) were converted to Ser (33). This mutant protein retains its ability to phosphorylate rhodopsin, albeit with a 5-fold higher K_m and 2-fold lower V_{max} compared with those of wild-type GRK6 (33). At ~48 h post-viral addition, 4–6 liters of infected cells were pelleted and resuspended in ~80 ml of ice-cold harvesting buffer containing 20 mM HEPES (pH 8.0), 100 mM NaCl, 5 mM EDTA, 5 mM EGTA, 2 mM dithiothreitol, 2 μM leupeptin, 2 mM lima bean trypsin inhibitor, 2 mM phenylmethylsulfonyl fluoride, and 2 mM tosylphenylalanyl chloromethyl ketone. The suspended cells were flash-frozen in liquid nitrogen and stored at −80 °C.

GRK6 was purified with the same protocol used for GRK2 (34), although GRK6 eluted from the final Source S column at ~130 mM NaCl, as opposed to 140 mM for GRK2. After gel filtration on a Superdex 200 16/600 preparative column pre-equilibrated with 20 mM HEPES (pH 8.0), 200 mM NaCl, and 2 mM dithiothreitol, GRK6 was pooled, concentrated to 12 mg/ml in a 50-kDa cutoff Centriprep filter (Millipore Corp.), and flash-frozen as 50-μl pellets in liquid nitrogen. The yield of pure GRK6 varied from 2 to 4 mg/liter of culture. Matrix-assisted laser desorption ionization mass spectrometry of the purified GRK6 protein yielded a molecular mass of 66,050 Da, slightly larger than expected (65,986 Da for acetylated, full-length, palmitoylation-deficient GRK6). This could indicate that GRK6 is post-translationally modified (*e.g.* via phosphorylation) when expressed in insect cells, as is GRK2 (7).

Crystallization—GRK6 was crystallized at 4 °C by hanging drop vapor diffusion in the presence of 2 mM $MgCl_2$ and 4 mM AMPPNP (final concentration). The presence of Mg^{2+}·AMPPNP was required for crystallization. The drop consisted of 1 μl of protein and 1 μl of well solution containing 100 mM succinic, malic, or citric acid (pH 4.9–5.1), 8.7–10.8% polyethylene glycol 3350, 4 mM $MgCl_2$, 5% ethylene glycol, and 500 mM NaCl. Crystals appeared in 5 days and grew over the course of 2–3 weeks as stacks of thin plates, with maximum dimensions of 1 × 0.3 × <0.05 mm. GRK6 crystals belong to the space group C2, with unit cell parameters $a = 120.2$, $b = 59.3$, and $c = 221.1$ Å and $\beta = 102.6°$, and contain two molecules in the asymmetric unit.

Data Collection and Structure Determination—Crystals were harvested by excising single plates with an eye knife (BD Biosciences) and transferred by CryoLoop into a cryoprotectant solution consisting of 20 mM HEPES (pH 8.0), 100 mM fumaric acid (pH 5.0), 400 mM NaCl, 1 mM dithiothreitol, 1 mM $MgCl_2$, 2 mM AMPPNP, 9.45% polyethylene glycol 3350, and 5% ethylene glycol. The crystals were then stepped through a gradient of ethylene glycol (3.25% increments up to 20% final) and flash-frozen in liquid nitrogen. Diffraction maxima were collected from crystals maintained at 100 K at Advanced Light Source beamline 8.3.1 on an ADSC Quantum 210 CCD detector. To avoid overlaps due to the long *c* cell axis, which was perpendicular to the plane of the crystal plates, it was necessary to crimp the base of the crystal mounting pin by ~45° while in the cryostream. Diffraction maxima were collected in two sweeps using 0.5° or 0.75° oscillations and 7- or 8-s exposures, respectively, for a total of 220° (368 images). During this process, the crystal was translated once in the beam to extend data collection. The data were reduced and scaled using ELVES (35) and associated programs from CCP4 (36) and solved by molecular replacement as implemented by the program Phaser (37), with the RH and kinase domains of GRK2 serving as search models (Protein Data Bank code 1OMW). Data sets were also collected from crystals soaked with 17 mM inositol 1,4,5-trisphosphate (IP_3) or 4 mM glycogen synthase kinase-3β (GSK3β) peptide (38). However, electron density was not observed for either molecule.

TABLE 1
Crystallographic data and refinement statistics
ALS, Advanced Light Source; r.m.s.d., root mean square deviation.

Crystallographic data	
X-ray source	ALS beamline 8.3.1
Wavelength (Å)	1.000
Resolution (Å)	2.6
Space group	C2
Cell constants	$a = 120.2$, $b = 59.3$, and $c = 221.1$ Å; $\beta = 102.6°$
Unique reflections	46,028 (6200)[a]
Average redundancy	3.8 (2.4)
R_{sym} (%)[b]	6.0 (51.1)
Completeness (%)	97.4 (90.7)
$\langle I \rangle / \langle \sigma_I \rangle$	9.3 (1.2)
Refinement statistics	
Refinement resolution (Å)	30 to 2.6
Total reflections used	45,986 (2895)[c]
Protein atoms	7995
Non-protein atoms	111
r.m.s.d. bond lengths (Å)	0.019
r.m.s.d. bond angles	1.8°
Estimated coordinate error (Å)	0.3
Ramachandran plot statistics (%)	
Most favored	90.4
Disallowed	0.0
R_{work}[d]	20.4 (32.9)
R_{free}[e]	24.3 (40.5)

[a] Numbers in parentheses correspond to the highest resolution shell of data (2.74 to 2.6 Å).
[b] $R_{sym} = \Sigma_{hkl} \Sigma_i |I(hkl)_i - I(hkl)| / \Sigma_{hkl} I(hkl)_i$, where $I(hkl)$ is the mean intensity of *i* reflections after rejections.
[c] Numbers in parentheses correspond to the highest resolution shell of data (2.67 to 2.6 Å).
[d] $R_{work} = \Sigma_{hkl} ||F_o(hkl)| - |F_c(hkl)|| / \Sigma_{hkl} |F_o(hkl)|$. No I/σ cutoff was used during refinement.
[e] 5% of the data set was excluded from refinement to calculate R_{free}.

Modeling—The molecular replacement model was refined for two cycles of simulated annealing and individual *B*-factor refinement in CNS_SOLVE (39) to reduce phase bias. The GRK6 model was then refined using both 2-fold NCS restraints and TLS groups in REFMAC5 (36). After each round of refinement, the model was manually fit into σ_A-weighted electron density maps using the molecular graphics program O (40). The stereochemistry of the model was monitored using PROCHECK (41). Atomic representations and electrostatic surfaces were created with PyMOL (42) and APBS (43).

Functional Analysis of the RH Dimerization Interface—To create the wild-type GRK6 expression vector pcDNA3-GRK6A, a 2038-bp fragment of human GRK6 cDNA (23) was excised with EcoRI and ligated into EcoRI-digested pcDNA3. Single mutations I39E, I165E, and F527D and double mutations I39E/I165E and I165E/F527D were made in pcDNA3-GRK6 using the QuikChange site-directed mutagenesis kit (Stratagene), and the full coding region of the resulting vector was sequenced for verification. GRK6 and its mutants were partially purified from transiently transfected COS-1 cells and analyzed in phosphorylation reactions following previously described procedures (44). After standardizing protein levels by Western analysis with a mouse anti-GRK4–6 monoclonal antibody (Upstate Cell Signaling Solutions), GRK6 and its mutants were assayed in phosphorylation reactions con-

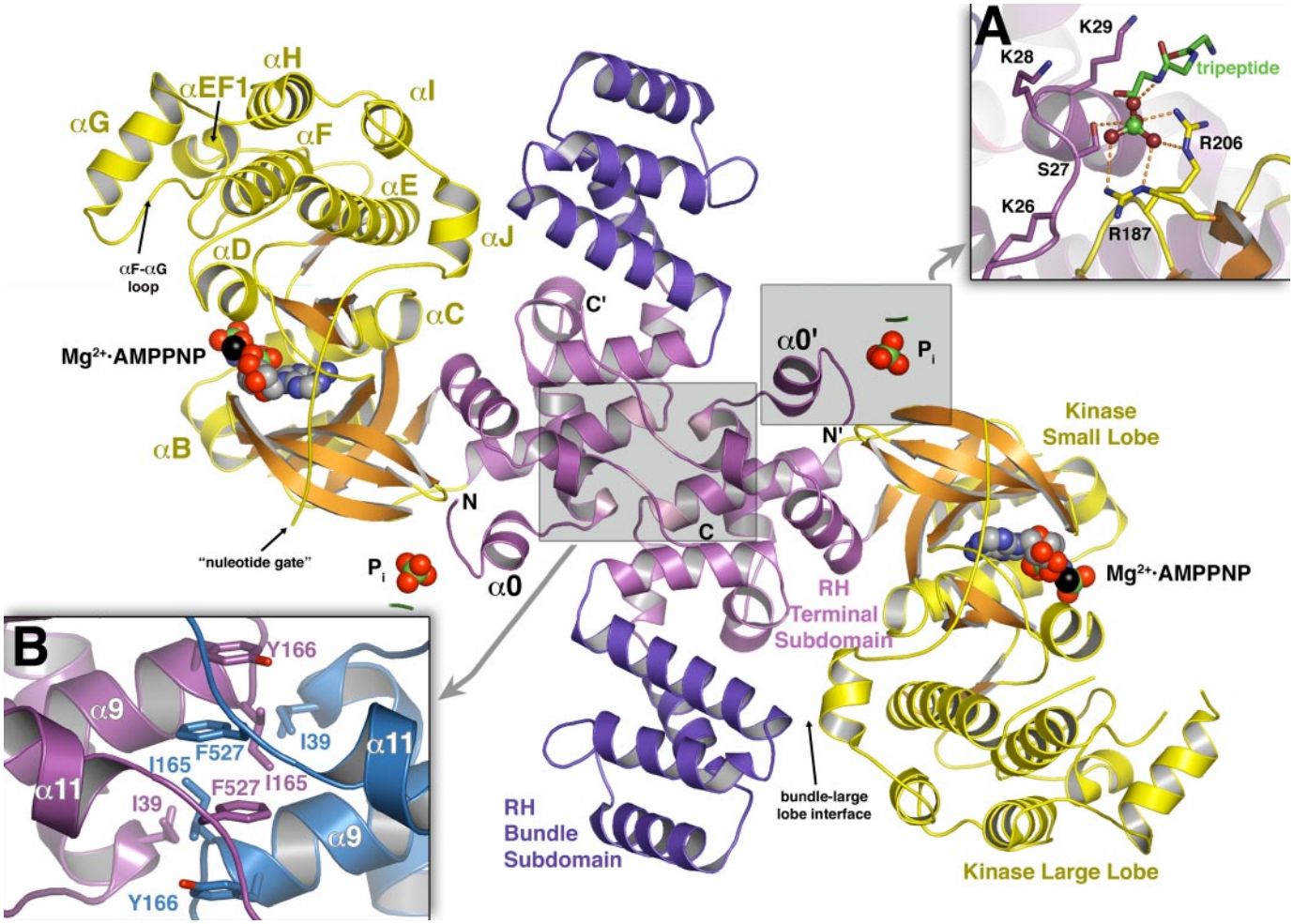

FIGURE 1. **The asymmetric unit of the GRK6 crystals contains a homodimer formed via a conserved surface of the RH domain.** Each GRK6 monomer consists of a bipartite RH domain containing 12 α helices. The terminal subdomain (*magenta*) forms the crystalline dimer interface and consists of the α0–α3 and α8–α11 helices. The bundle subdomain forms an antiparallel four-helix bundle (*dark purple*) and consists of the remaining helices (α4–α7). The α1–α9 helices are homologous to those in the RH domains of RGS proteins. Compared with the structure of GRK2 (10), GRK6 has an additional N-terminal helix (α0) and shorter α5 and α11 helices. The GRK6 kinase domain (*yellow* α helices and *orange* β sheets) is composed of small and large lobes and is inserted between the α9 and α10 helices of the RH domain. Mg^{2+}·AMPPNP (*spheres*) is bound within each active site. *Gray boxes* correspond to regions magnified in the *insets*. *Inset A*, a polyvalent anion (modeled as P_i) is bound to a putative phospholipid-binding site at the N terminus of GRK6 composed by residues from the α0 helix and the small lobe of the kinase domain. Density large enough for a tripeptide (shown with *green* carbons) also interacts with the anion. Potential hydrogen bonds and salt bridges are shown as *dashed lines*. *Inset B*, the RH dimer interface buries 2700 $Å^2$ of surface area. Residues that form the hydrophobic core of the interface are shown, including an interdigitated aromatic stack between the side chains of Tyr^{166} and Phe^{527} from each subunit. The backbone nitrogen and carbonyl groups of Phe^{527} also form β sheet-like hydrogen bonds across the dimer interface. Nitrogen atoms are colored *blue*, oxygen *red*, phosphate *green*, and magnesium *black*. Carbon atoms are colored according to the domain in which they are found, except for those in AMPPNP, which are *gray*.

taining light-exposed, urea-stripped rod outer segments. Parallel reactions performed in the dark did not reveal rhodopsin phosphorylation. Chemiluminescence detection (Western blotting) and PhosphorImager analysis (phosphorylation assay) were performed using a Typhoon imaging system and analyzed with ImageQuant software. Statistical analysis was performed with repeated measures analysis of variance.

Sedimentation Equilibrium—Palmitoylation-deficient GRK6 samples were prepared at three concentrations (corresponding to A_{280} = 0.3, 0.5, and 0.6) in 20 mM HEPES (pH 8.0), 200 mM NaCl, and 2 mM dithiothreitol and analyzed in an An50Ti rotor at 4 °C at three rotor speeds (10,000, 15,000 and 25,000 rpm) in a Beckman XL-1 analytical ultracentrifuge. Data were analyzed using Ultrascan Version 7.2 software (available at www.ultrascan.uthscsa.edu) by modeling the sample as a single ideal solute with a calculated partial specific volume of 0.735 ml/g to obtain a buoyant molecular mass of 60 ± 1 kDa and a variance of 1.4×10^{-5}. This result suggests that GRK6 (expected molecular mass of 66 kDa) is predominantly monomeric at each concentration tested. Gel filtration analysis performed at a higher concentration (40 μM) was also consistent with a monomeric protein.

RESULTS

The crystal structure of the human GRK6·AMPPNP complex was determined using diffraction data extending to 2.6-Å spacings, with phases provided by molecular replacement (Table 1). Two monomers of GRK6 (chains A and B) are present in the asymmetric unit of the crystals and form a homodimer that buries 2700 $Å^2$ of accessible surface area (Fig. 1). The final model contains residues 24–474 and 492–532 in chain A and residues 24–387, 391–473, and 492–535 in chain B (supplemental Fig. S1). Mass spectroscopic analysis of the protein used for crystallization suggests that the missing regions are disordered and not proteolyzed. The missing residues from positions 474/475 to 491 in each chain correspond to the so-called "nucleotide gate" region of the kinase domain (45), which was similarly disordered in structures of GRK2. A polyvalent anion modeled as inorganic phosphate is bound to residues near the basic N terminus of the protein (Fig. 1), which may represent part of an anionic phospholipid-binding site in each monomer (46). Discontinuous but strong electron density was observed adjacent to the phosphate anion in each chain and was tentatively modeled

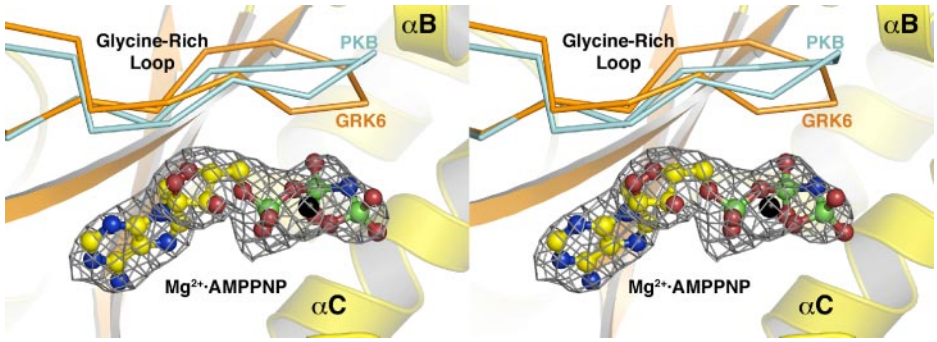

FIGURE 2. **Stereo view of Mg^{2+}·AMPPNP bound in the active site of GRK6.** A σ_A-weighted $|F_o| - |F_c|$ omit map contoured at 3 σ is shown as a *gray cage*. Mg^{2+} (*black sphere*) is bound between the α- and γ-phosphates. The glycine-rich loop (or P-loop) of GRK6 is shown as a C^{α} trace. The analogous loop of PKB (*cyan*) (38) was superimposed and appears shifted (upwards in this view) away from the nucleotide-binding site and the large lobe relative to that of GRK6.

as residues 14–16 of each GRK6 monomer due to its proximity to Lys^{24}, the first identified residue in each chain. However, this density could also correspond to residues from the C terminus of each chain, which are also nearby and disordered.

The region of greatest sequence conservation among GRKs is the kinase domain, which spans residues 180–507 in GRK6. As in other protein kinases, the catalytic site of the GRK6 kinase domain is situated in a cleft between a "small lobe" (residues 180–318 and 492–507) and a "large lobe" (residues 319–471) (Fig. 1). Despite the presence of Mg^{2+}·AMPPNP in the active site (Fig. 2), the kinase domain of GRK6 crystallized in an "open," inactive conformation with a disordered nucleotide gate. This is atypical for an AGC kinase, wherein the binding of nucleotide analogs correlates well with kinase domain closure and ordering of the nucleotide gate region (15). Upon superimposing the small lobes of GRK6 and GRK2, their large lobes are rotated ~10° with respect to each other. However, neither assumes a more "closed" conformation because both require an ~18° rotation to match the AMPPNP-bound conformation of PKB (supplemental Fig. S2) (38). In either case, the axis of rotation required to achieve the closed conformation is roughly parallel to the αD helix of the kinase domain, passing adjacent to GRK6 Ser^{328} (GRK2 Ser^{334}) within the active site.

The structure of AMPPNP bound in the GRK6 active site allows comparison of a GRK catalytic site with other AGC kinases (38, 47). As in PKA or PKB, the catalytic lysine residue (Lys^{215}) interacts with the α- and β-phosphates of the ATP analog, and the purine ring fits snuggly into a hydrophobic specificity pocket. Only weak density for one of the two expected magnesium ions is observed in GRK6, perhaps because active-site residues donated by the large lobe (*e.g.* Asn^{316} and Asp^{329}, both of which coordinate magnesium) are displaced due to the open conformation of the kinase domain. Thus, the active-site cleft presented by nucleotide-bound GRKs is substantially broader than that of nucleotide-bound PKA or PKB (Fig. 3, compare *A* and *D*). Furthermore, the position of the triphosphate tail and associated glycine-rich "P-loop" is shifted by 2–3 Å toward the large lobe relative to that of AMPPNP-bound PKA or PKB (Fig. 2) and has the same conformation as it does in the nucleotide-free structures of GRK2. Therefore, no evidence exists for a conformational change in this loop upon binding ATP, as there is in PKA and other protein kinases (15, 48). The structural basis for this difference is not clear, although we speculate that it could be due to substitutions within the adjacent αB helix.

The αD–αE and αF–αG loops of the GRK6 large lobe correspond to loops in other characterized AGC kinases that form the walls of the peptide-binding channel. In GRK6, these loops are 2 and 1 residue(s) longer, respectively, than in GRK2 (supplemental Fig. S1) and adopt strikingly different conformations. In the GRK6 A chain, ^{387}QRKKK^{391} of the αF–αG loop obstruct the end of the peptide channel where the N terminus of peptides bind to PKA and PKB. In contrast, ^{388}RKK^{390} in the B chain are disordered. This difference probably results from the facts that the A chain is generally better ordered than the B chain and that the A chain αF–αG loop is directly stabilized by a crystal contact. It is possible that this contact could also influence the structure of the αF–αG loop. However, the positions of residues 387 and 391 in the B chain strongly suggest that their intervening residues also most occupy the peptide channel. Thus, either GRK6 binds substrates in a manner that is not strictly analogous to how PKB binds the GSK3β peptide (Fig. 3) (38), or the αF–αG loop adopts an alternative conformation upon substrate binding. Assuming that residues 387–391 are displaced upon substrate/receptor binding, the peptide channel of GRK6 appears to be only mildly acidic compared with those of PKA and PKB (Fig. 3, *B* and *D*). In contrast, the peptide channel of GRK2 is strikingly basic and favors peptide substrates with acidic residues N-terminal to the phosphorylation site (Fig. 3*C*) (49). Interestingly, region 387–391 also appears to serve as a DNA-binding nuclear localization sequence in GRK5 and potentially GRK6 (50).

The N-terminal portion of the GRK6 RH domain consists of 12 α helices associated into "bundle" (α4–α7) and "terminal" (α0–α3 and α8–α11) subdomains (Fig. 4*A* and supplemental Fig. S1). Superposition of the GRK2 and GRK6 RH domains (root mean square deviation of 1.4 Å for 144 structurally equivalent C^{α} atoms) demonstrates that these subdomains are oriented similarly with respect to each other and thus are distinct from RH domains of the RGS protein family wherein the two subdomains are twisted ~22° relative to those of GRKs. The GRK2 and GRK6 RH domains are most divergent at their N termini. In GRK2, this region forms an interface with its PH domain. In GRK6, an additional helix is found at the N terminus (α0), which provides additional bridging contacts between the RH and kinase domains and includes a run of basic residues previously implicated in binding phosphatidylinositol 4,5-bisphosphate and calmodulin (Figs. 1 and 4*A*) (46, 51). Thus, in both the GRK2 and GRK4 subfamilies, the N-terminal region of the RH domain appears to have evolved to interact with and/or support the unique membrane-binding determinants that are characteristic of each subfamily.

The GRK6 RH domain does not have structural determinants currently known to be required for binding Gα subunits in either GRK2 or the RGS protein family. Specifically, α5 of GRK6 is approximately two turns shorter than that of GRK2 and thereby lacks residues analogous to those critical for GRK2 binding to $G\alpha_q$ (Fig. 4, *A* and *B*; and supplemental Fig. S1) (22, 52). Furthermore, the α5–α6 loop, a critical determinant for binding $G\alpha_i$, $G\alpha_t$, or $G\alpha_q$ subunits in RGS proteins (53, 54), has a distinct structure in GRK6, implying that the GRK6 RH domain cannot serve as a GTPase-activating protein for Gα subunits, at least in a manner that would be analogous to RGS proteins.

However, the RH domain of GRK6 does form a conserved extensive

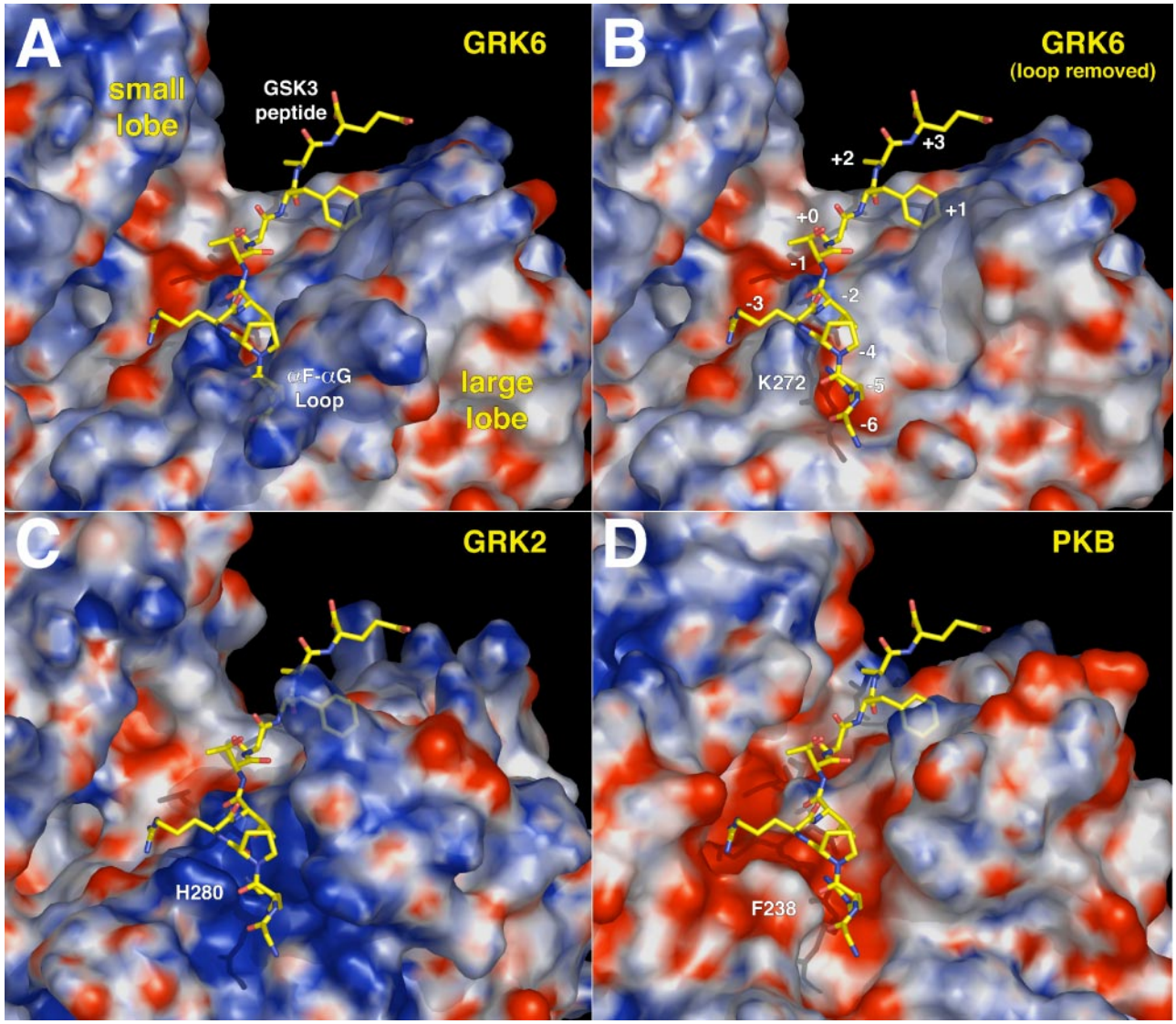

FIGURE 3. **Comparison of the GRK6, GRK2, and PKB peptide-binding channels.** The large lobes of the kinase domains of GRK6, GRK2 (10), and PKB (38) are aligned, and the bound GSK3β peptide (stick model with *yellow* carbons) from the PKB structure (Protein Data Bank code 1O6K) was then mapped onto the GRK6 and GRK2 large lobes. The accessible surface of each kinase domain is shown and is colored from -7 (*red*, acidic) to $+7$ (*blue*, basic) kT/e^{-}. *A*, the N-terminal region of the GRK6 channel is obstructed by residues 387–391 of the αF–αG loop. *B*, the GRK6 channel with residues 387–391 removed. The resulting channel is similar to that of PKA or PKB (compare with *D*), except that the channel has a lysine (Lys^{214}) at a position occupied by histidine (His^{280}) in GRK2 (*C*) and by phenylalanine (Phe^{328}) in PKB (*D*). This gives the GRK6 channel a more neutral character compared with the PKB channel. Residues in the GSK3β peptide are labeled -6 through $+3$ with respect to the site of phosphorylation ($+0$). GRK6 Lys^{214} has steric overlap with the peptide as modeled. *C*, the GRK2 channel is strikingly basic. This is due to the loss of key acidic residues relative to other AGC kinases (supplemental Fig. S1). Unlike in GRK6, the channel appears unobstructed and compatible with peptides that adopt the same backbone configuration as the GSK3β peptide in the PKB·GSK3 peptide complex. *D*, the PKB channel favors basic residues N-terminal to the site of phosphorylation in its substrates. Note that the closure of the PKB kinase domain creates a comparatively narrow cleft between the large and small lobes. The corresponding cleft of GRKs remains open whether bound to nucleotide (*A* and *B*) or not (*C*).

protein dimer interface using a region similar to that used by the RH domain of p115RhoGEF to bind a $G\alpha_{i/13}$ chimera (Figs. 1 and Fig. 4*A* and supplemental Fig. S1) (55). The interface buries 2700 $Å^2$ of accessible surface area and features a short β sheet interaction between the C termini of each GRK6 monomer and an interdigitated aromatic stack involving the side chains of Phe^{527} and Tyr^{166} and their dimer equivalents (Figs. 1 (*inset B*) and 4*A*). Ile^{39} (α1) and Ile^{165} (α9) also contribute their side chains to the core of the interface. Hydrophobic residues are conserved at each of these positions in GRK1 and GRK5, whereas most are conserved in GRK7 and GRK4 (supplemental Fig. S1). Interestingly, p115RhoGEF Met^{165}, which docks into the effector site of $G\alpha_{13}$ (55), projects from the RH domain from a position that is topologically equivalent to GRK6 Ile^{165}. However, there is currently no evidence for a direct interaction between GRK6 and Gα subunits (19).

Despite the extent of the dimer interface and the conservation of residues that form it, palmitoylation-deficient GRK6 behaves as a monomer in solution both as determined by size exclusion chromatography and sedimentation equilibrium analysis (data not shown). However, dimerization might still occur at the membrane surface where the local concentration of GRK6 is high or upon encountering substrates, such as activated GPCRs, that are potentially dimeric (56, 57). We therefore tested whether the hydrophobic residues buried within the observed dimer interface are required for receptor phosphorylation. The I39E, I165E, and F527D site-directed mutants were created to inhibit dimer formation by burying charge and/or creating steric collisions. The mutants were expressed in COS-1 cells, and all phosphorylated light-activated rhodopsin to roughly the same extent as wild-type GRK6 (data not shown). Because single mutations alone may not be sufficient to disrupt such a large interface, two double mutants of GRK6 (I39E/I165E and I165E/F527D) were also assessed for their ability to phosphorylate

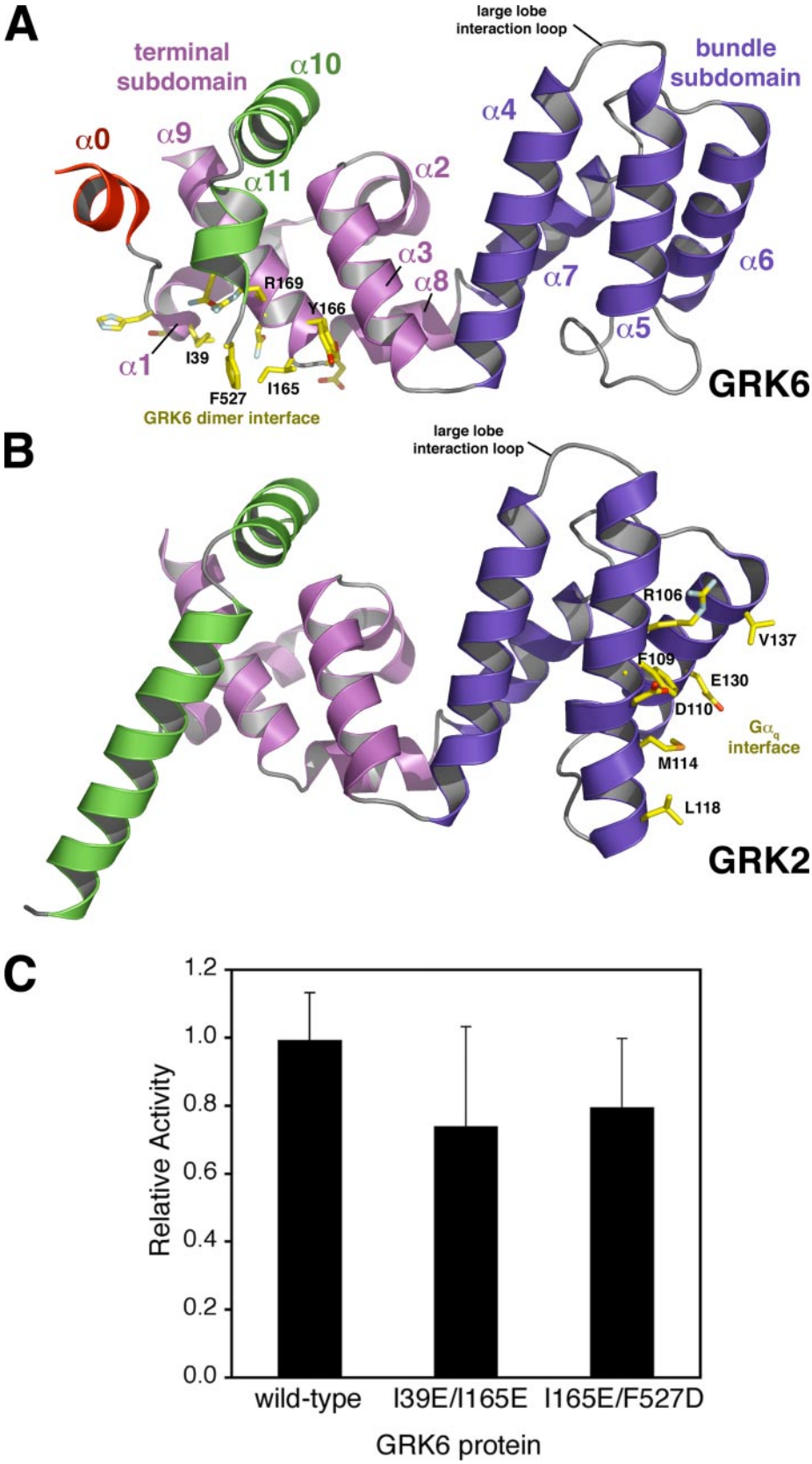

FIGURE 4. **The GRK6 RH domain contains a protein interaction surface.** *A*, the GRK6 RH domain. The α1–α9 helices (colored according to their respective subdomains) are conserved in all RH domains, whereas the α10 and α11 helices (*green*) are characteristic of the GRK family. The side chains of residues that form the core of the GRK6 dimer interface (see Fig. 1) are shown as stick models with *yellow* carbons. *B*, the GRK2 RH domain. The relatively longer α5 helix of GRK2 helps to form the $G\alpha_q$-binding site (side chains with *yellow* carbons), whereas the longer α11 helix joins the RH and PH domains and contains basic residues that likely interact with the membrane surface. *C*, mutation of buried hydrophobic residues of the GRK6 interface does not abrogate phosphorylation of light-activated rhodopsin in rod outer segments. Statistical analysis was performed on three experiments in which two to three independent transfection samples were prepared. $p < 0.05$ only when comparing the wild type with the I39E/I165E mutant.

rhodopsin. These mutations only slightly reduced receptor phosphorylation (Fig. 4*C*). Although we cannot prove that these mutations prevent dimerization of GRK6, it is clear that the residues tested are not required for the phosphorylation of activated GPCRs under our assay conditions, regardless of whether they are involved in protein-protein interactions at the cell membrane.

The GRK6 RH and kinase domains are intimately associated through two contact surfaces that together bury 2000 $Å^2$ of accessible surface

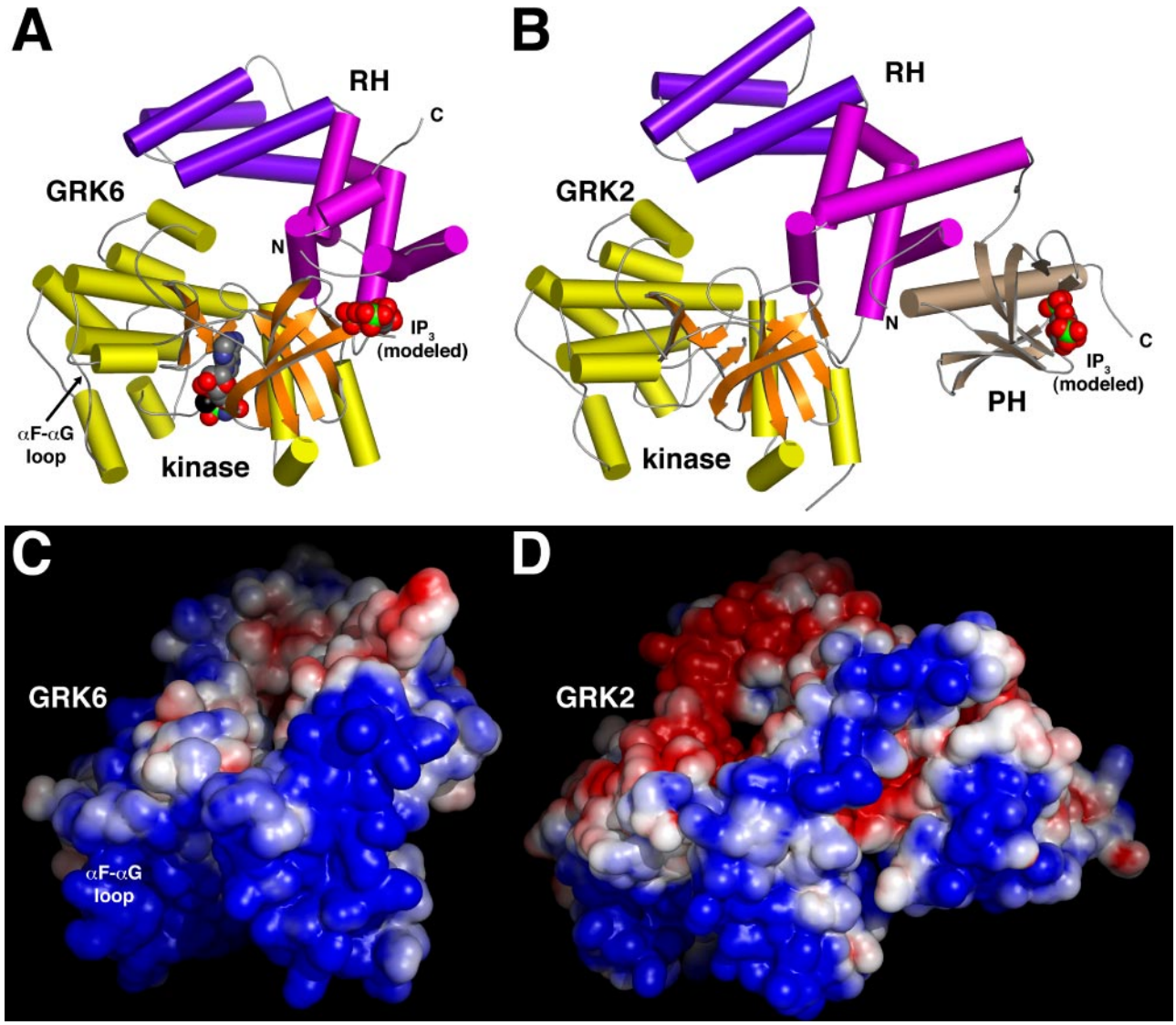

FIGURE 5. **The membrane-binding determinants in GRK6 and GRK2 are arranged similarly.** GRK6 (*A*) and GRK2 (*B*) are expected to maintain similar orientations with respect to the membrane of the cell. For reference, IP_3 has been docked with the protein to demarcate the expected phospholipid-binding sites. In GRK6, the 5′-phosphate of IP_3 was superimposed on the polyvalent anion site observed in the crystal structure (Fig. 1). In GRK2, IP_3 was docked onto the PH domain using the structure of the phospholipase Cδ1 PH domain·IP_3 complex (Protein Data Bank code 1DJX) as a model. The C terminus of GRK6 is palmitoylated in the wild-type enzyme. Although it is disordered in our structure, it will be close to the expected membrane plane. Solvent-accessible surfaces of GRK6 (*C*) and GRK2 (*D*) are shown in the same orientation as in *A*. The surface is colored by the electrostatic potential ($\pm 3\ kT/e^-$). Both GRK6 and GRK2 have similar basic regions (*blue*) forming a flat surface that we believe will interact with the membrane plane. The αF–αG loop of GRK6, which occupies part of the peptide-binding channel and purportedly serves as a nuclear localization sequence (50), is also intensely basic, but below the expected membrane plane.

area (Figs. 1 and 5), 300 Å^2 more surface area than in GRK2. The largest contact surface (1560 Å^2) is formed by the α0 and α10 helices from the RH terminal subdomain packing against the small lobe from the kinase domain. The smaller contact surface (440 Å^2) is formed between the α4–α5 loop of the RH bundle subdomain and the αJ region of the kinase domain large lobe. This interface is approximately twice as large in GRK6 than in GRK2 and involves several interdomain hydrogen bonds, a salt bridge, and hydrophobic interactions that appear to be conserved throughout the GRK1 and GRK4 subfamilies (supplemental Fig. S1). The bipartite interaction between the RH and kinase domains therefore appears to be conserved in all GRKs.

Despite similarities in their interdomain contacts, the RH-kinase domain core of GRK6 is different in conformation than that of GRK2. The binding of AMPPNP may have induced this conformational change in GRK6, although it could also simply reflect structural divergence between the GRK2 and GRK4 subfamilies. Upon superposition of the kinase domain small lobes of GRK2 and GRK6, the RH domain of GRK6 is rotated ~12° with respect to that of GRK2, with the apparent axis of rotation running roughly through the centers of the terminal small lobe and bundle large lobe interfaces. This axis of rotation is roughly parallel to that which relates the large lobes of the GRK2 and GRK6 kinase domains (supplemental Fig. S2). Because these rotations are of similar magnitude and direction, the observed changes in the orientation of the RH domain and the large lobe of GRK6 with respect to those of GRK2 appear to be coupled.

The association of GRK6 with the cell membrane is mediated in part by the palmitoylation of cysteine residues that lie in a C-terminal region that is not ordered in our crystal structure (58). In addition, GRK4 subfamily members possess a putative phosphatidylinositol 4,5-bisphosphate-binding site at the N terminus involving a sequence that packs between the RH and kinase domains in the structure of GRK6 (^{22}NRKGKSKK^{29}) (supplemental Fig. S1) (46). All but the first two residues of this sequence are observed in our crystal structure. Strong tetrahedral electron density is observed in close proximity to these res-

idues and is attributed to either the imidophosphate or sulfonate of AMPPNP or HEPES, respectively, used during crystallization. The polyvalent anion, modeled as P_i (Fig. 1, *inset A*), is bound via hydrogen bonds or salt bridges with Ser^{27}, Arg^{187}, and Arg^{206}, the latter two residues being from the β sheet of the kinase small lobe. These residues are invariant in the GRK4 subfamily (supplemental Fig. S1). The tripeptide we tentatively modeled as residues 14–16 (Fig. 1) additionally appears to donate a backbone hydrogen bond. Given the proximity of the polyanion to Ser^{27}, we considered whether this residue might be phosphorylated, especially because Ser^{29} of GRK2 is phosphorylated by protein kinase C (6), and Ser^{21} of GRK1 is autophosphorylated (59). However, GRK2 Ser^{29} is not structurally equivalent to either of these residues (supplemental Fig. S1), and a phosphoserine at GRK6 position 27 is not compatible with our electron density maps and would not have reasonable stereochemistry. We instead propose that the anion occupies part of a binding site for an anionic phospholipid, such as the 4′- or 5′-phosphates of phosphatidylinositol 4,5-bisphosphate.

Remarkably, the position of the putative phosphatidylinositol 4,5-bisphosphate-binding site and the disordered N and C termini of GRK6, which contain additional membrane-binding determinants, are positioned in roughly the same topological position with respect to the RH-kinase domain core as the GRK2 PH domain, and both enzymes form a relatively flat and positively charged surface on their RH and kinase domains that we speculate will interact with biological membranes (Fig. 5). Thus, despite the lack of sequence and structural conservation at the N and C termini of GRKs, the catalytic and membrane-targeting sites are similarly arranged in both the GRK4 and GRK2 subfamilies. It seems likely that all GRKs will interact with membranes in a similar fashion, with their kinase active sites in close proximity to the membrane surface to receive their receptor substrates.

DISCUSSION

GRK2 is an important target for treatment of heart failure (60), whereas GRK6 is a target for treatment of addiction and Parkinson disease (28, 29). Comparison of the GRK2 and GRK6 structures reveals features of their kinase domains that could be exploited to increase the selectivity of drugs for GRKs over other AGC kinases. Because nucleotide binding does not induce domain closure in either GRK2 or GRK6 (supplemental Fig. S2), and the GRK P-loop appears to be locked in a conformation resembling that of nucleotide-bound (and activated) PKA or PKB, the GRK active-site cleft presents a unique landscape for potential inhibitors compared with other AGC kinases. There are also obvious subfamily-specific differences between the GRK6 and GRK2 kinase domains. Their peptide-binding channels have profoundly different electrostatic character (Fig. 3), in accordance with previous biochemical studies showing that GRK4 subfamily members prefer neutral peptide substrates, and GRK2 acidic ones (49, 61). The αF–αG loop obstructs one end of the peptide channel in GRK6 (Fig. 3). It is possible that, in the GRK4 and GRK1 subfamilies, this loop autoinhibits kinase activity until an activated GPCR is encountered. Alternatively, polypeptide substrates might bind to GRK6 in a different way than predicted from the peptide complexes of PKA and PKB.

The RH-kinase domain cores of GRK2 and GRK6 have structural differences not only within their RH and kinase domains, but also in how these domains are oriented with respect to each other. Despite this, a similar bipartite interaction is maintained between the RH and kinase domains in both enzymes, indicating an evolutionarily conserved role for the interface. One role could be to stabilize the kinase small lobe in its active state, in part because the terminal subdomain-small lobe interface fixes in place the so-called "hydrophobic motif" at the C terminus of the kinase domain. In PKB and protein kinase C, this motif stably associates with the small lobe only after phosphorylation, which is required for full kinase activity in these proteins (62, 63). Because GRK kinase domains have thus far proved resistant to crystallization in a closed state similar to AMPPNP-bound PKB, another role of the RH-kinase domain interface may be to stabilize the inactive conformation of the kinase domain, similar to how SH2 (Src homology 2) domain restrains the kinase large lobe in Src family kinases (12, 14). Disruption of the bundle subdomain-large lobe interface may therefore be required for kinase domain closure and activation. Alternatively, the RH bundle subdomain could simply "track" with the large lobe during closure, as does the A helix of PKA, which likewise bridges the lobes of its kinase domain (15). Finally, because the RH domain interacts with and/or supports the various membrane-binding determinants in both GRK2 and GRK6, another role of the RH-kinase domain interface may be to fix the positions of these elements with respect to the kinase active site. Indeed, the topological locations of the membrane-binding determinants in GRK2 and GRK6 are strikingly similar despite their structural divergence (Fig. 5).

Intriguingly, GRK6 crystallized as a dimer using a surface of its RH domain that is highly conserved in both the GRK4 and GRK1 subfamilies (Fig. 1 and supplemental Fig. S1). Because palmitoylation-deficient GRK6 is a monomer in solution, dimerization clearly resulted from the high protein concentration within the GRK6 crystals. However, the conservation, extent, and hydrophobicity of the surface used for dimerization still point toward a functional role. Although the crystalline GRK6 dimer is not compatible with how we believe GRK2 interacts with membranes (Fig. 5), it remains possible that GRK1 and GRK4 family members interact with membranes or their receptor targets as the observed dimer in a different orientation than GRK2 (*e.g.* using the surface shown in Fig. 1). It is also possible that a dimer form of GRK6 is required for cellular functions other than receptor phosphorylation (50) or that the interface used for dimerization in the crystal is used to bind another, as of yet unidentified, protein target in cells.

The GRK kinase domain has now been observed to adopt an open, presumably inactive conformation in eight independent crystal structures: one in the GRK2·G$\beta\gamma$ structure (10), four in the GRK2 structure (9), one in the Gα_q·GRK2·G$\beta\gamma$ structure (11), and two in the GRK6·AMPPNP structure. Therefore, this open conformation is neither a crystallization artifact nor a GRK2-specific feature. Furthermore, the GRK6·AMPPNP structure demonstrates that the binding of adenine nucleotides does not lead to kinase domain closure. Because phosphorylation of the GRK kinase domain is not required for activation, as it is in other AGC kinases (62), all requirements for activation appear to be fulfilled in our GRK structures except for kinase domain closure. We therefore propose that receptor binding provides sufficient free energy to induce this closure, which either directly involves or leads to the ordering of the nucleotide gate and the extreme N terminus of the enzyme (the first 15–17 amino acids). These elements are not observed in the GRK2 and GRK6 crystal structures. The nucleotide gate is expected to make contacts within the active-site cleft and perhaps with peptide substrates, as it does in PKA. The GRK N terminus is required for efficient receptor phosphorylation and thereby implicated in receptor or phospholipid binding or in the structural transition from the inactive to active state of the kinase (8, 64, 65). Future studies of GRKs in an active, "receptor-bound" conformation will shed additional light on the functional roles of these structural elements and the molecular basis for activation of GRKs by GPCRs.

Acknowledgments—We thank J. Holten, T. Alber, and other members of the Advanced Light Source beamline 8.3.1 user support team for creative crystallographic devices and assistance that facilitated collection of GRK6 diffraction data. We thank Q. Li, T. Ludlam, and P. Singh for technical assistance and R. Sterne-Marr for rhodopsin used in some of the phosphorylation assays.

REFERENCES

1. Pitcher, J. A., Freedman, N. J., and Lefkowitz, R. J. (1998) *Annu. Rev. Biochem.* **67,** 653–692
2. Krupnick, J. G., and Benovic, J. L. (1998) *Annu. Rev. Pharmacol. Toxicol.* **38,** 289–319
3. Premont, R. T., Macrae, A. D., Aparicio, S. A., Kendall, H. E., Welch, J. E., and Lefkowitz, R. J. (1999) *J. Biol. Chem.* **274,** 29381–29389
4. Siderovski, D. P., Hessel, A., Chung, S., Mak, T. W., and Tyers, M. (1996) *Curr. Biol.* **6,** 211–212
5. Benovic, J. L., De Blasi, A., Stone, W. C., Caron, M. G., and Lefkowitz, R. J. (1989) *Science* **246,** 235–240
6. Krasel, C., Dammeier, S., Winstel, R., Brockmann, J., Mischak, H., and Lohse, M. J. (2001) *J. Biol. Chem.* **276,** 1911–1915
7. Pitcher, J. A., Tesmer, J. J., Freeman, J. L., Capel, W. D., Stone, W. C., and Lefkowitz, R. J. (1999) *J. Biol. Chem.* **274,** 34531–34534
8. Noble, B., Kallal, L. A., Pausch, M. H., and Benovic, J. L. (2003) *J. Biol. Chem.* **278,** 47466–47476
9. Lodowski, D. T., Barnhill, J. F., Pyskadlo, R. M., Ghirlando, R., Sterne-Marr, R., and Tesmer, J. J. (2005) *Biochemistry* **44,** 6958–6970
10. Lodowski, D. T., Pitcher, J. A., Capel, W. D., Lefkowitz, R. J., and Tesmer, J. J. (2003) *Science* **300,** 1256–1262
11. Tesmer, V. M., Kawano, T., Shankaranarayanan, A., Kozasa, T., and Tesmer, J. J. (2005) *Science* **310,** 1686–1690
12. Xu, W., Harrison, S. C., and Eck, M. J. (1997) *Nature* **385,** 595–602
13. Williams, J. C., Weijland, A., Gonfloni, S., Thompson, A., Courtneidge, S. A., Superti-Furga, G., and Wierenga, R. K. (1997) *J. Mol. Biol.* **274,** 757–775
14. Sicheri, F., Moarefi, I., and Kuriyan, J. (1997) *Nature* **385,** 602–609
15. Taylor, S. S., Yang, J., Wu, J., Haste, N. M., Radzio-Andzelm, E., and Anand, G. (2004) *Biochim. Biophys. Acta* **1697,** 259–269
16. Haga, K., and Haga, T. (1992) *J. Biol. Chem.* **267,** 2222–2227
17. Pitcher, J. A., Inglese, J., Higgins, J. B., Arriza, J. L., Casey, P. J., Kim, C., Benovic, J. L., Kwatra, M. M., Caron, M. G., and Lefkowitz, R. J. (1992) *Science* **257,** 1264–1267
18. Koch, W. J., Inglese, J., Stone, W. C., and Lefkowitz, R. J. (1993) *J. Biol. Chem.* **268,** 8256–8260
19. Carman, C. V., Parent, J. L., Day, P. W., Pronin, A. N., Sternweis, P. M., Wedegaertner, P. B., Gilman, A. G., Benovic, J. L., and Kozasa, T. (1999) *J. Biol. Chem.* **274,** 34483–34492
20. Sallese, M., Mariggio, S., D'Urbano, E., Iacovelli, L., and De Blasi, A. (2000) *Mol. Pharmacol.* **57,** 826–831
21. Usui, H., Nishiyama, M., Moroi, K., Shibasaki, T., Zhou, J., Ishida, J., Fukamizu, A., Haga, T., Sekiya, S., and Kimura, S. (2000) *Int. J. Mol. Med.* **5,** 335–340
22. Sterne-Marr, R., Tesmer, J. J., Day, P. W., Stracquatanio, R. P., Cilente, J. A., O'Connor, K. E., Pronin, A. N., Benovic, J. L., and Wedegaertner, P. B. (2003) *J. Biol. Chem.* **278,** 6050–6058
23. Benovic, J. L., and Gomez, J. (1993) *J. Biol. Chem.* **268,** 19521–19527
24. Loudon, R. P., Perussia, B., and Benovic, J. L. (1996) *Blood* **88,** 4547–4557
25. Lombardi, M. S., Kavelaars, A., Schedlowski, M., Bijlsma, J. W., Okihara, K. L., Van de Pol, M., Ochsmann, S., Pawlak, C., Schmidt, R. E., and Heijnen, C. J. (1999) *FASEB J.* **13,** 715–725
26. Willets, J. M., Challiss, R. A., and Nahorski, S. R. (2003) *Trends Pharmacol. Sci.* **24,** 626–633
27. Gainetdinov, R. R., Premont, R. T., Bohn, L. M., Lefkowitz, R. J., and Caron, M. G. (2004) *Annu. Rev. Neurosci.* **27,** 107–144
28. Gainetdinov, R. R., Bohn, L. M., Sotnikova, T. D., Cyr, M., Laakso, A., Macrae, A. D., Torres, G. E., Kim, K. M., Lefkowitz, R. J., Caron, M. G., and Premont, R. T. (2003) *Neuron* **38,** 291–303
29. Bezard, E., Gross, C. E., Qin, L., Gurevich, V. V., Benovic, J. L., and Gurevich, E. V. (2005) *Neurobiol. Dis.* **18,** 323–335
30. Fong, A. M., Premont, R. T., Richardson, R. M., Yu, Y. R., Lefkowitz, R. J., and Patel, D. D. (2002) *Proc. Natl. Acad. Sci. U. S. A.* **99,** 7478–7483
31. Kavelaars, A., Vroon, A., Raatgever, R. P., Fong, A. M., Premont, R. T., Patel, D. D., Lefkowitz, R. J., and Heijnen, C. J. (2003) *J. Immunol.* **171,** 6128–6134
32. Vroon, A., Heijnen, C. J., Raatgever, R., Touw, I. P., Ploemacher, R. E., Premont, R. T., and Kavelaars, A. (2004) *J. Leukocyte Biol.* **75,** 698–704
33. Loudon, R. P., and Benovic, J. L. (1997) *J. Biol. Chem.* **272,** 27422–27427
34. Lodowski, D. T., Barnhill, J. F., Pitcher, J. A., Capel, W. D., Lefkowitz, R. J., and Tesmer, J. J. (2003) *Acta Crystallogr. Sect. D Biol. Crystallogr.* **59,** 936–939
35. Holton, J., and Alber, T. (2004) *Proc. Natl. Acad. Sci. U. S. A.* **101,** 1537–1542
36. Winn, M. D. (2003) *J. Synchrotron Radiat.* **10,** 23–25
37. Storoni, L. C., McCoy, A. J., and Read, R. J. (2004) *Acta Crystallogr. Sect. D Biol. Crystallogr.* **60,** 432–438
38. Yang, J., Cron, P., Good, V. M., Thompson, V., Hemmings, B. A., and Barford, D. (2002) *Nat. Struct. Biol.* **9,** 940–944
39. Brünger, A. T., Adams, P. D., Clore, G. M., DeLano, W. L., Gros, P., Grosse-Kunstleve, R. W., Jiang, J. S., Kuszewski, J., Nilges, M., Pannu, N. S., Read, R. J., Rice, L. M., Simonson, T., and Warren, G. L. (1998) *Acta Crystallogr. Sect. D Biol. Crystallogr.* **54,** 905–921
40. Jones, T. A., Zou, J. Y., Cowan, S. W., and Kjeldgaard, M. (1991) *Acta Crystallogr. Sect. A* **47**, 110–119
41. Laskowski, R. A., MacArthur, M. W., Moss, D. S., and Thornton, J. M. (1993) *J. Appl. Crystallogr.* **26,** 283–291
42. DeLano, W. L. (2002) *The PyMOL Molecular Graphics System*, DeLano Scientific LLC, San Carlos, CA
43. Baker, N. A., Sept, D., Joseph, S., Holst, M. J., and McCammon, J. A. (2001) *Proc. Natl. Acad. Sci. U. S. A.* **98,** 10037–10041
44. Pronin, A. N., Loudon, R. P., and Benovic, J. L. (2002) *Methods Enzymol.* **343,** 547–559
45. Narayana, N., Cox, S., Nguyen-huu, X., Ten Eyck, L. F., and Taylor, S. S. (1997) *Structure* (*Lond.*) **5,** 921–935
46. Pitcher, J. A., Fredericks, Z. L., Stone, W. C., Premont, R. T., Stoffel, R. H., Koch, W. J., and Lefkowitz, R. J. (1996) *J. Biol. Chem.* **271,** 24907–24913
47. Bossemeyer, D., Engh, R. A., Kinzel, V., Ponstingl, H., and Huber, R. (1993) *EMBO J.* **12,** 849–859
48. Huse, M., and Kuriyan, J. (2002) *Cell* **109,** 275–282
49. Onorato, J. J., Palczewski, K., Regan, J. W., Caron, M. G., Lefkowitz, R. J., and Benovic, J. L. (1991) *Biochemistry* **30,** 5118–5125
50. Johnson, L. R., Scott, M. G., and Pitcher, J. A. (2004) *Mol. Cell. Biol.* **24,** 10169–10179
51. Pronin, A. N., Satpaev, D. K., Slepak, V. Z., and Benovic, J. L. (1997) *J. Biol. Chem.* **272,** 18273–18280
52. Day, P. W., Carman, C. V., Sterne-Marr, R., Benovic, J. L., and Wedegaertner, P. B. (2003) *Biochemistry* **42,** 9176–9184
53. Tesmer, J. J. G., Berman, D. M., Gilman, A. G., and Sprang, S. R. (1997) *Cell* **89,** 251–261
54. Srinivasa, S. P., Watson, N., Overton, M. C., and Blumer, K. J. (1998) *J. Biol. Chem.* **273,** 1529–1533
55. Chen, Z., Singer, W. D., Sternweis, P. C., and Sprang, S. R. (2005) *Nat. Struct. Mol. Biol.* **12,** 191–197
56. Terrillon, S., and Bouvier, M. (2004) *EMBO Rep.* **5,** 30–34
57. Milligan, G. (2004) *Mol. Pharmacol.* **66,** 1–7
58. Stoffel, R. H., Randall, R. R., Premont, R. T., Lefkowitz, R. J., and Inglese, J. (1994) *J. Biol. Chem.* **269,** 27791–27794
59. Palczewski, K., Buczylko, J., Van Hooser, P., Carr, S. A., Huddleston, M. J., and Crabb, J. W. (1992) *J. Biol. Chem.* **267,** 18991–18998
60. Koch, W. J. (2004) *Mol. Cell. Biochem.* **263,** 5–9
61. Kunapuli, P., Onorato, J. J., Hosey, M. M., and Benovic, J. L. (1994) *J. Biol. Chem.* **269,** 1099–1105
62. Newton, A. C. (2002) *Biochem. J.* **370,** 361–371
63. Frodin, M., Antal, T. L., Dummler, B. A., Jensen, C. J., Deak, M., Gammeltoft, S., and Biondi, R. M. (2002) *EMBO J.* **21,** 5396–5407
64. Yu, Q. M., Cheng, Z. J., Gan, X. Q., Bao, G. B., Li, L., and Pei, G. (1999) *J. Neurochem.* **73,** 1222–1227
65. Palczewski, K., Buczylko, J., Lebioda, L., Crabb, J. W., and Polans, A. S. (1993) *J. Biol. Chem.* **268,** 6004–6013